Geometry-Aware Manifold Trajectory Modeling for Task fMRI Activation Mapping

Yueran Li[1], Xinle Chang[1], Yang Yang[1], Yu Zhao[2], and Jingyong Su[1⋆]

[1] Harbin Institute of Technology (Shenzhen), Shenzhen, Guangdong, China
[2] West China Hospital of Sichuan University, Chengdu, Sichuan, China
sujingyong@hit.edu.cn

Abstract. Functional magnetic resonance imaging (fMRI) measures task-evoked neural activity through blood-oxygen-level-dependent (BOLD) signals and enables activation mapping to localize task-related brain responses. Conventional activation mapping typically relies on the general linear model (GLM), which assumes linearity and a predefined hemodynamic response function (HRF). However, mounting evidence indicates that BOLD responses are nonlinear and state-dependent. Meanwhile, the high dimensionality and low signal-to-noise ratio of fMRI further challenge the linear assumption. These limitations motivate a neural-manifold view, in which high dimensional task dynamics evolve on a low-dimensional state space. We propose a geometry-aware manifold trajectory modeling framework that represents task-related activity as structured trajectories. The framework identifies a central baseline cluster, computes geodesic distances from each embedded frame to this cluster along the manifold trajectory graph, and converts them into vertex-wise activation maps via the proposed Manifold Geodesic-based Similarity (MGS) without HRF fitting. Using the Human Connectome Project (HCP) motor-task fMRI dataset, we uncover a petal-like looped trajectory, indicating a reproducible low-dimensional organization of task-evoked dynamics. At the individual-level, MGS robustly recovers canonical motor activations despite substantial single-subject fMRI noise. At the group-level, compared with HRF-based GLM, MGS yields more discriminative activation patterns and highlights task-related effects less emphasized by GLM, demonstrating the advantage of geometry-aware manifold trajectories for task fMRI activation mapping. Code is available at https://github.com/PCMLYR/ManifoldTraj_MGS

Keywords: Brain manifold · fMRI · Geodesic distance · Brain activation mapping · General linear model.

1 Introduction

Functional Magnetic Resonance Imaging (fMRI) infers task-evoked brain activity through the blood-oxygen-level-dependent (BOLD) signal, whose contrast reflects changes in deoxyhemoglobin driven by neurovascular coupling [22]. A core

⋆ Corresponding author

objective of task fMRI is activation mapping: identifying brain regions whose BOLD time series are modulated by externally controlled cognitive states so that condition-specific functional organization can be localized and compared across subjects [1]. The prevailing analysis framework is the General Linear Model (GLM) [10], which assumes that task effects add linearly after convolution with a canonical hemodynamic response function (HRF) [4, 17]. While effective in many settings, GLM is sensitive to HRF mismatch and latency variability across regions and individuals [26]. More fundamentally, the transformation from neural activity to BOLD is not strictly linear and time-invariant: hemodynamic saturation, refractory interactions, and nonlinear vascular dynamics can violate the canonical HRF assumption and blur condition selectivity [11]. These limitations motivate activation measures that are less dependent on a fixed HRF model and can better accommodate nonlinear task-evoked dynamics [17].

A second bottleneck is that whole-brain BOLD data are intrinsically high dimensional and low signal-to-noise: each frame is a large activity vector, yet task-relevant structure is weak relative to physiological and measurement variability, making inference challenging under purely local modeling [8]. Task fMRI analyses can also be sensitive to analytic choices and may exhibit limited test–retest reliability in commonly used activation measures [3, 9]. These nonlinearities motivate a manifold viewpoint: task-evoked brain states may evolve on a low-dimensional nonlinear neural manifold as smooth trajectories that depart from and return to an intrinsic baseline [12, 24, 21, 25, 16]. A broad class of nonlinear embeddings has been used to recover such geometry from high-dimensional observations, including LLE [23], diffusion maps [7], t-SNE [18], UMAP [19], and PHATE [20]. Recent advances such as T-PHATE [6] explicitly exploit autocorrelative temporal structure to denoise fMRI time series and uncover interpretable state trajectories. Notably, these studies often reveal recurrent or loop-like trajectories that align with cognitive conditions [20, 6, 16]. However, these loops are frequently treated as qualitative signatures for visualization or segmentation, while their geometric meaning is rarely translated into a principled, geometry-aware activation statistic, particularly one that measures progression along the manifold (e.g., via geodesic distance) rather than in the ambient space.

Here we present a geometry-aware, data-driven framework for brain surface task fMRI activation mapping and demonstrate its utility on Human Connectome Project (HCP) motor-task fMRI dataset. Rather than relying on a fixed HRF model, we characterize task-evoked dynamics as structured state evolution on a low-dimensional manifold, where successive frames form a petal-like looped trajectory with condition-aligned excursions. This geometric view exposes an intrinsic task baseline region (dominated by fixation and quiescent transitions) and yields a temporally resolved distance-to-baseline signature that tracks task engagement. Leveraging this signature, we propose the Manifold Geodesic-based Similarity (MGS), which reliably recovers canonical motor somatotopy while producing more compact and condition-selective activation patterns than HRF-constrained GLM, and additionally highlights task-relevant effects that can be weak under purely linear, voxel-wise modeling.

In summary, our contributions are threefold: (1) We propose a geometry-aware manifold trajectory modeling framework that characterizes task fMRI as structured state evolution on a learned low-dimensional manifold. (2) We introduce a geodesic distance-to-baseline geometric measure on the learned manifold trajectory to provide a model-light reference for task engagement and subsequent activation inference. (3) Using HCP motor-task fMRI, we uncover reproducible petal-like looped manifold trajectories with a central baseline cluster and demonstrate that the resulting MGS-based maps recover canonical motor organization while yielding more compact and discriminative group-level patterns than conventional HRF-based GLM.

2 Materials and Methods

2.1 Dataset and Preprocessing

We analyzed WU-Minn Human Connectome Project Young Adult (HCP-YA) 2025 release [27] resting-state and motor task fMRI data from a subset of 100 unrelated healthy adults (22–35 years; sex-balanced), acquired on a 3T Siemens Connectome Skyra (TR=0.72 s; 2 mm isotropic). Data were processed using the HCP minimal preprocessing pipeline [15] and the 2025 release denoising outputs (sICA+FIX with reclean and temporal ICA; spin-echo field-map assistance) [13, 14], yielding CIFTI grayordinate BOLD time series. We additionally applied 4-mm FWHM smoothing and vertex-wise mean-centering, without temporal filtering. The motor task followed the HCP design [5] with five cue-driven

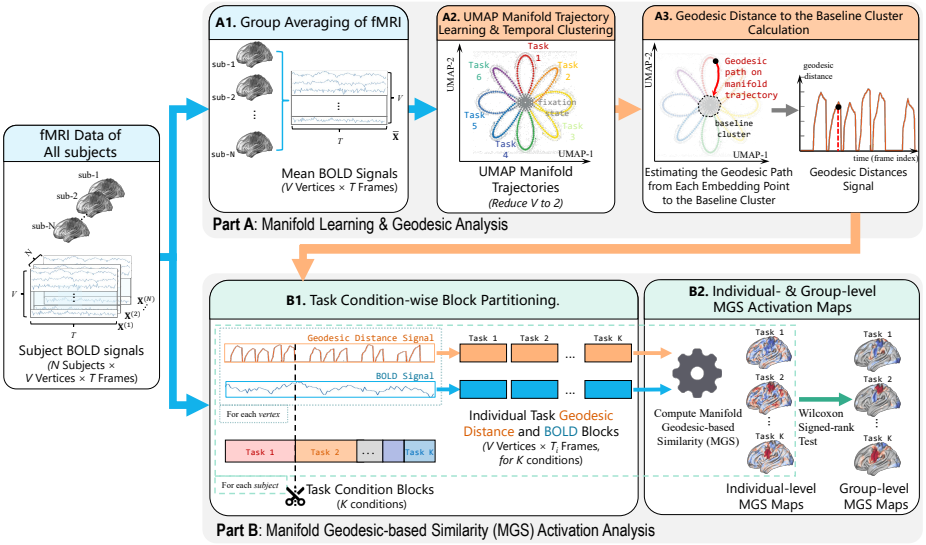

Fig. 1. Overview of the proposed manifold trajectory learning and MGS activation mapping framework.

movements (left/right hand, left/right foot, tongue). All subjects completed two phase-encoding runs (LR/RL), each with 10 task blocks (2 per condition) separated by 15-s fixation.

2.2 Manifold Learning and Geodesic Analysis

Group Averaging of fMRI. Let $\mathbf{X}^{(n)} \in \mathbb{R}^{V\times T}$ denote the preprocessed task fMRI time series of subject n ($n = 1, \ldots, N$), where V is the number of brain surface vertices and T is the number of task frames. We first computed a group-averaged sequence $\bar{\mathbf{X}} = \frac{1}{N}\sum_{n=1}^{N} \mathbf{X}^{(n)} \in \mathbb{R}^{V\times T}$ as shown in Fig. 1(A1), and treated each frame t as a V-dimensional vector $\bar{\mathbf{x}}_t = \bar{\mathbf{X}}_{:,t} \in \mathbb{R}^V$.

UMAP Manifold Trajectory Learning and Temporal Clustering. The shared low-dimensional manifold representation was learned by mapping $\bar{\mathbf{x}}_t$ to $\mathbf{y}_t \in \mathbb{R}^2$ using UMAP [19] (task frames only; LR/RL concatenated; $n_{\text{neighbors}} = 40$; standardized Euclidean distance) as shown in Fig. 1(A2). The ordered set $\Gamma = \{\mathbf{y}_t\}_{t=1}^{T}$, with consecutive points connected by time index, defines a manifold trajectory capturing whole-brain state evolution during the task. This trajectory serves as the geometric substrate for subsequent distance-to-baseline computation.

We identified recurrent manifold states by clustering $\{\mathbf{y}_t\}$ using Density-based Merging (DBM) [28]. Among the resulting clusters, we defined the task baseline cluster C_{base} as the union of the one or two DBM clusters whose centroids are closest to the embedding center; if only one such cluster exists, we use that cluster alone. C_{base} is the central, high-density region of the embedding dominated by fixation and run-onset quiescent frames.

Geodesic Distance to the Baseline Cluster Calculation. We represented the ordered embeddings $\{\mathbf{y}_t\}_{t=1}^{T}$ as a trajectory graph on the learned manifold by connecting consecutive frames in time, and the geodesic was approximated by temporal adjacency. The resulting trajectory graph has edge weights $\ell_t = \|\mathbf{y}_{t+1} - \mathbf{y}_t\|_2$ between adjacent nodes. Specifically, for each frame t, we quantify the deviation of its temporal embedding point from the within-task baseline (baseline cluster C_{base}) by the shortest path from this point to the baseline cluster on the trajectory graph, i.e., the geodesic distance to baseline, defined as:

$$d_G(t) = \min_{t' \in C_{\text{base}}} \text{dist}(t, t'), \tag{1}$$

where $\text{dist}(t, t')$ is the shortest-path distance on the undirected trajectory graph from temporal embedding point t to t' (can be traversed forward or backward in time), so that each frame is assigned its own along-trajectory geodesic path and distance to the baseline cluster. We computed $d_G(t)$ on the manifold trajectory learned from the group-averaged fMRI and reused it for all subjects

to obtain a stable, shared geometric feature of task-evoked dynamics as illustrated in Fig. 1(A3). Thus, individual-level variability was captured only through vertex-wise BOLD blocks in later steps.

2.3 Manifold Geodesic-based Similarity (MGS) Activation Analysis

Task Condition-wise Block Partitioning. To align task events with hemodynamic responses, we used a fixed shift of 6 frames (≈4.32 s for the HCP dataset) as a coarse latency alignment rather than HRF fitting. Using the delay-shifted labels, each subject's vertex-wise time series was segmented into condition blocks, denoted $\mathbf{f}_{v,k,b}^{(n)}$ for vertex v, condition k, and repetition b as shown in Fig. 1(B1). Using the same time windows, we extracted the matched geodesic distance-to-baseline signal $\mathbf{d}_{G,k,b}$ calculated by Eq.(1).

Individual- and Group-Level MGS Activation Maps Calculation. We define the Manifold Geodesic-based Similarity (MGS) as the alignment between a BOLD block and its corresponding manifold-distance pattern. As Fig. 1(B2) shows, for each block, we mapped distances to a bounded weight vector $w(\mathbf{x}) = 1 - \exp(-\mathbf{x})$ (element-wise) and computed a block score by the inner product between the ℓ_2-normalized BOLD block and $w(\mathbf{d}_{G,k,b})$. Averaging over the B_k repetitions of condition k gives

$$\mathrm{MGS}_{v,k}^{(n)} = \frac{1}{B_k} \sum_{b=1}^{B_k} \left\langle \frac{\mathbf{f}_{v,k,b}^{(n)}}{\|\mathbf{f}_{v,k,b}^{(n)}\|_2 + \varepsilon},\ w(\mathbf{d}_{G,k,b}) \right\rangle, \tag{2}$$

where ε is a small constant for numerical stability. For each condition k, $\mathrm{MGS}_{:,k}^{(n)} \in \mathbb{R}^V$ forms an individual-level brain activation map used for subsequent group inference and comparison with GLM-based activation.

For each subject n and vertex v, we computed a resting-state MGS map $\mathrm{MGS}_{v,\mathrm{rest}}^{(n)}$ from the subject's resting-state fMRI by segmenting it into pseudo-blocks that match the motor-task block length (and number of blocks) and applying Eq.(2) with the same distance templates $\mathbf{d}_{G,k,b}$ in the same block order as the task data. No random sampling was used for selecting resting-state pseudo-blocks.

For each task condition k, we then formed a within-subject contrast

$$\Delta MGS_{v,k}^{(n)} = \mathrm{MGS}_{v,k}^{(n)} - \mathrm{MGS}_{v,\mathrm{rest}}^{(n)}. \tag{3}$$

Group-level task modulation was assessed at each (v, k) by testing $H_0 : \Delta MGS_{v,k} = 0$ across subjects using a two-sided Wilcoxon signed-rank test (non-parametric, without assuming normality). Multiple comparisons across vertices were controlled separately for each condition using the Benjamini–Hochberg FDR [2] procedure, declaring significance at $p_{FDR} < 0.05$. Significant vertices were labeled as *activated* if $\mathrm{median}_n(\Delta MGS_{v,k}^{(n)}) > 0$ and *suppressed* if $\mathrm{median}_n(\Delta MGS_{v,k}^{(n)}) < 0$.

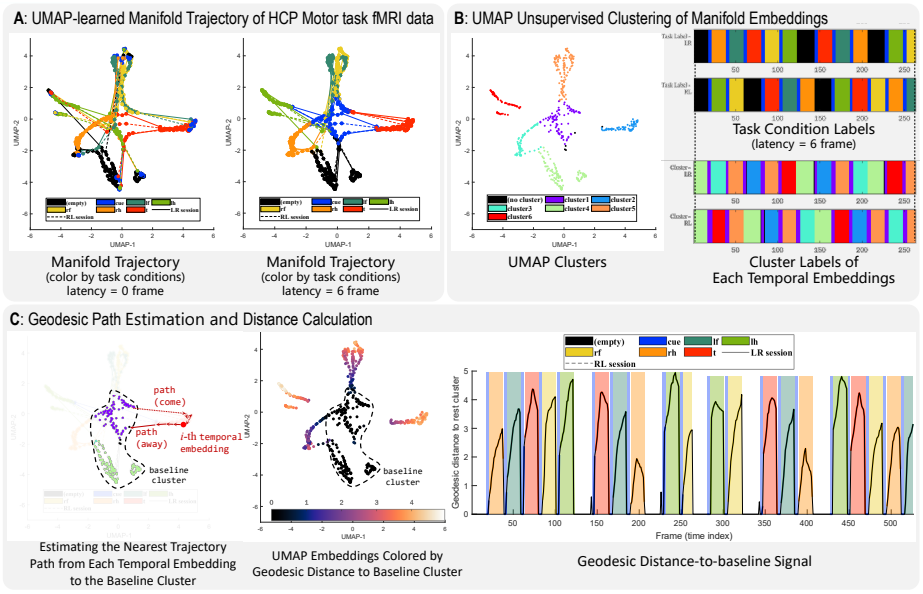

Fig. 2. Manifold trajectory, clustering, and geodesic distance to baseline. (A) Manifold trajectories of group-averaged HCP motor-task fMRI colored by condition labels (0-frame vs. 6-frame delay shift). **(B)** Clusters in the embedding (left) and the corresponding LR/RL temporal sequences of condition labels and cluster assignments (right). **(C)** Diagram of frame-wise geodesic path estimation (left), embeddings colored by distance-to-baseline (middle), and the resulting frame-wise geodesic distance signal over time (right; shaded bands denote task blocks).

3 Experimental Results

3.1 Manifold Trajectory Reveals Condition-aligned Petals and Geodesic Distance Signal

Figure 2 summarizes the group-level manifold geometry learned from HCP motor-task fMRI and motivates our distance-based analysis. Fig. 2A shows the 2D UMAP embedding of the group-averaged time series, where successive frames trace a petal-like looped trajectory. With nominal task timing (0-frame latency), points from the same condition are partially mixed across petals, consistent with hemodynamic delay; applying a 6-frame shift ($\sim$4.32 s) yields substantially more condition-coherent, petal-specific structure (Fig. 2A, right). Unless otherwise noted, all subsequent analyses use the 6-frame–shifted timing.

This structure also emerges without task labels: unsupervised DBM clustering produces compact, well-separated manifold clusters (Fig. 2B) that closely correspond to the shifted condition labels over time. Using two central clusters as a baseline region, we compute for each point the shortest along-trajectory path length back to baseline, producing a geodesic distance-to-baseline signal

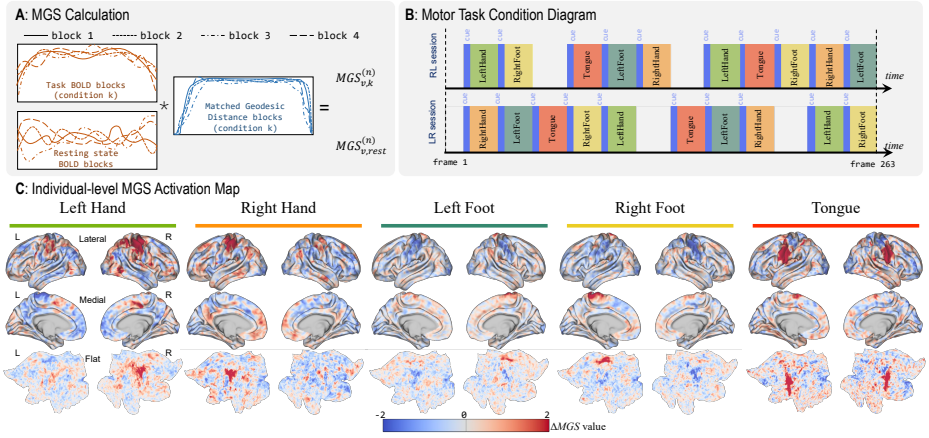

Fig. 3. MGS calculation and individual-level ΔMGS map for motor task. **(A)** MGS calculation procedure. Condition-wise MGS is obtained by matching task BOLD blocks with the corresponding geodesic distance signal blocks. **(B)** Motor task condition diagram. Block design for concatenated LR and RL runs showing cue and effector conditions (left/right hand, left/right foot, tongue). **(C)** Individual-level MGS activation maps of five motor task conditions. (lateral/medial/flat views; colors indicate signed ΔMGS value).

(Fig. 2C). The resulting rise-and-return profiles track departures from and returns to baseline during task engagement and serve as a temporally resolved geometric summary for subsequent condition-wise similarity analysis and activation mapping.

3.2 Individual-level MGS Activation Maps

Figure 3 summarizes individual-level MGS results for the HCP Motor task. Briefly, MGS is computed condition-wise by matching each task BOLD block with the corresponding geodesic-distance block (Fig. 3A), using the motor design timing across concatenated LR/RL runs (Fig. 3B). Representative individual-level MGS maps (Fig. 3C) show expected motor-system organization. Hand conditions localize to the contralateral precentral/postcentral hand knob, foot conditions emphasize the medial sensorimotor representation near the paracentral lobule, and tongue movements engage ventral sensorimotor/peri-opercular regions, demonstrating individual-level somatotopy and lateralization. These results indicate that MGS preserves physiologically plausible activation patterns at the individual-level that can be carried forward to group-level inference.

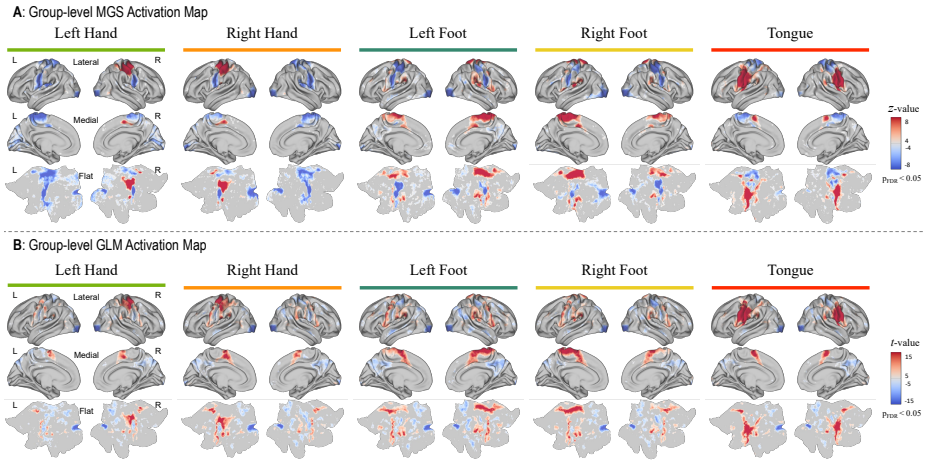

Fig. 4. Group-level activation detection maps for motor task: MGS vs. GLM. **(A)** MGS group maps (signed z-values; $p_{FDR} < 0.05$) and **(B)** GLM group maps (t-values; $p_{FDR} < 0.05$) for left/right hand, left/right foot, and tongue conditions.

3.3 Group-level MGS Activation Detection and Comparison with GLM

Figure 4 contrasts group-level activation maps obtained with the proposed MGS framework versus a conventional GLM analysis for each motor effector. Across conditions, both approaches recover the canonical motor network organization: strong, contralateral sensorimotor effects for left/right hand around the precentral–postcentral area, medial wall engagement for foot movements near the paracentral lobule, and ventral sensorimotor/peri-opercular involvement for tongue. These results indicate that MGS preserves the expected task-specific somatotopy at the group-level.

Notably, the MGS maps (Fig. 4A) are more spatially compact and condition-selective, showing less diffuse effects outside primary sensorimotor regions than the GLM maps (Fig. 4B), which may reflect shared variance across blocks and sensitivity to HRF specification. Moreover, MGS provides a signed task–rest modulation (activation vs. suppression), whereas GLM inference is tied to a fixed HRF-convolved regressor and in practice often emphasizes positive responses under common modeling choices. Together, these properties suggest that MGS can yield sharper, more discriminative group-level maps by exploiting an intrinsic, manifold-derived distance-to-baseline reference rather than relying solely on an explicit HRF model.

4 Conclusion

In this work, we presented a manifold-geometric framework for task fMRI activation mapping. On HCP motor-task data, UMAP embeddings reveal robust petal-

like looped trajectories, where delay-shifted labels improve condition alignment and expose BOLD latency, and identify condition-specific clusters together with a central baseline cluster as an intrinsic baseline. We quantify task engagement by geodesic distance-to-baseline along the trajectory graph and introduce Manifold Geodesic-based Similarity (MGS) to translate these geometric excursions into vertex-wise activation estimates for both individual- and group-level analyses. MGS recovers canonical motor somatotopy while producing more compact and condition-selective maps than GLM, and it additionally highlights task-relevant effects that can be weak under HRF-constrained linear modeling. Limitations include evaluation on a single paradigm and reliance on a group-level manifold. Future work will extend to additional tasks and develop subject-adaptive manifolds and geodesic statistics.

Acknowledgments. This work was supported by National Natural Science Foundation of China (grant No. 62376068, U24A20340, 32361143787), by Guangdong Basic and Applied Basic Research Foundation (grant No. 2023B1515120065).

Disclosure of Interests. The authors have no competing interests to declare that are relevant to the content of this article.

References

1. Barch, D.M., Burgess, G.C., Harms, M.P., Petersen, S.E., Schlaggar, B.L., Corbetta, M., Glasser, M.F., Curtiss, S., Dixit, S., Feldt, C., et al.: Function in the human connectome: task-fmri and individual differences in behavior. NeuroImage **80**, 169–189 (2013)
2. Benjamini, Y., Hochberg, Y.: Controlling the false discovery rate: a practical and powerful approach to multiple testing. Journal of the Royal Statistical Society: Series B (Methodological) **57**(1), 289–300 (1995)
3. Botvinik-Nezer, R., Holzmeister, F., Camerer, C.F., Dreber, A., Huber, J., Johannesson, M., Kirchler, M., Iwanir, R., Mumford, J.A., Adcock, R.A., et al.: Variability in the analysis of a single neuroimaging dataset by many teams. Nature **582**(7810), 84–88 (2020)
4. Boynton, G.M., Engel, S.A., Glover, G.H., Heeger, D.J.: Linear systems analysis of functional magnetic resonance imaging in human v1. Journal of Neuroscience **16**(13), 4207–4221 (1996)
5. Buckner, R.L., Krienen, F.M., Castellanos, A., Diaz, J.C., Yeo, B.T.: The organization of the human cerebellum estimated by intrinsic functional connectivity. Journal of Neurophysiology **106**(5), 2322–2345 (2011)
6. Busch, E.L., Huang, J., Benz, A., Wallenstein, T., Lajoie, G., Wolf, G., Krishnaswamy, S., Turk-Browne, N.B.: Multi-view manifold learning of human brain-state trajectories. Nature Computational Science **3**, 240–253 (2023)
7. Coifman, R.R., Lafon, S.: Diffusion maps. Applied and Computational Harmonic Analysis **21**(1), 5–30 (2006)
8. Cunningham, J.P., Yu, B.M.: Dimensionality reduction for large-scale neural recordings. Nature Neuroscience **17**(11), 1500–1509 (2014)

9. Elliott, M.L., Knodt, A.R., Ireland, D., Morris, M.L., Poulton, R., Ramrakha, S., Sison, M.L., Moffitt, T.E., Caspi, A., Hariri, A.R.: What is the test-retest reliability of common task-functional mri measures? new empirical evidence and a meta-analysis. Psychological Science **31**(7), 792–806 (2020)
10. Friston, K.J., Holmes, A.P., Worsley, K.J., Poline, J.P., Frith, C.D., Frackowiak, R.S.: Statistical parametric maps in functional imaging: a general linear approach. Human Brain Mapping **2**(4), 189–210 (1994)
11. Friston, K.J., Mechelli, A., Turner, R., Price, C.J.: Nonlinear responses in fmri: the balloon model, volterra kernels, and other hemodynamics. NeuroImage **12**(4), 466–477 (2000)
12. Gallego, J.A., Perich, M.G., Miller, L.E., Solla, S.A.: Neural manifolds for the control of movement. Neuron **94**(5), 978–984 (2017)
13. Glasser, M.F., Coalson, T.S., Bijsterbosch, J.D., Harrison, S.J., Harms, M.P., Anticevic, A., Van Essen, D.C., Smith, S.M.: Using temporal ica to selectively remove global noise while preserving global signal in functional mri data. NeuroImage **181**, 692–717 (2018)
14. Glasser, M.F., Coalson, T.S., Bijsterbosch, J.D., Harrison, S.J., Harms, M.P., Anticevic, A., Van Essen, D.C., Smith, S.M.: Classification of temporal ica components for separating global noise from fmri data: Reply to power. NeuroImage **197**, 435–438 (2019)
15. Glasser, M.F., Sotiropoulos, S.N., Wilson, J.A., Coalson, T.S., Fischl, B., Andersson, J.L., Xu, J., et al.: The minimal preprocessing pipelines for the human connectome project. NeuroImage **80**, 105–124 (2013)
16. Iyer, K.K., Hwang, K., Hearne, L.J., Muller, E., D'Esposito, M., Shine, J.M., Cocchi, L.: Focal neural perturbations reshape low-dimensional trajectories of brain activity supporting cognitive performance. Nature Communications **13**(1), 4 (2022)
17. Lindquist, M.A.: The statistical analysis of fmri data. Statistical Science **23**(4), 439–464 (2008)
18. van der Maaten, L., Hinton, G.: Visualizing data using t-sne. Journal of Machine Learning Research **9**, 2579–2605 (2008)
19. McInnes, L., Healy, J., Melville, J.: Umap: Uniform manifold approximation and projection for dimension reduction. arXiv preprint arXiv:1802.03426 (2018)
20. Moon, K.R., van Dijk, D., Wang, Z., Gigante, S., Burkhardt, D.B., Chen, W.S., Yim, K., et al.: Visualizing structure and transitions in high-dimensional biological data. Nature Biotechnology **37**, 1482–1492 (2019)
21. Nick, Q., Gale, D.J., Areshenkoff, C., De Brouwer, A., Nashed, J., Wammes, J., Zhu, T., Flanagan, R., Smallwood, J., Gallivan, J.: Reconfigurations of cortical manifold structure during reward-based motor learning. Elife **12**, RP91928 (2024)
22. Ogawa, S., Lee, T.M., Kay, A.R., Tank, D.W.: Brain magnetic resonance imaging with contrast dependent on blood oxygenation. Proceedings of the National Academy of Sciences **87**(24), 9868–9872 (1990)
23. Roweis, S.T., Saul, L.K.: Nonlinear dimensionality reduction by locally linear embedding. Science **290**(5500), 2323–2326 (2000)
24. Rué-Queralt, J., Stevner, A., Tagliazucchi, E., Laufs, H., Kringelbach, M.L., Deco, G., Atasoy, S.: Decoding brain states on the intrinsic manifold of human brain dynamics across wakefulness and sleep. Communications Biology **4**(1), 854 (2021)
25. Song, H., Shim, W.M., Rosenberg, M.D.: Large-scale neural dynamics in a shared low-dimensional state space reflect cognitive and attentional dynamics. Elife **12**, e85487 (2023)

26. Uruñuela, E., Gonzalez-Castillo, J., Zheng, C., Bandettini, P., Caballero-Gaudes, C.: Whole-brain multivariate hemodynamic deconvolution for functional mri with stability selection. Medical Image Analysis **91**, 103010 (2024)
27. Van Essen, D.C., Smith, S.M., Barch, D.M., Behrens, T.E., Yacoub, E., Ugurbil, K., Consortium, W.M.H., et al.: The wu-minn human connectome project: an overview. NeuroImage **80**, 62–79 (2013)
28. Walther, G., Zimmerman, N., Moore, W., Parks, D., Meehan, S., Belitskaya, I., Pan, J., Herzenberg, L.: Automatic clustering of flow cytometry data with density-based merging. Advances in Bioinformatics **2009**(1), 686759 (2009)